Soft Matter

PAPER

View Article Online
View Journal | View Issue

Cite this: *Soft Matter*, 2023, 19, 5513

Pickering emulsions stabilised with oligoglycine-functionalised nanodiamond as a model system for ocular drug delivery applications†

Zhiwei Huang,[a] Roman V. Moiseev,[bc] Solomon S. Melides,[a] Wooli Bae,[a] Izabela Jurewicz,[a] Vitaliy V. Khutoryanskiy[bc] and Joseph L. Keddie *[a]

Oil-in-water emulsions, stabilised with conventional surfactants, are commonly used in eye drops for ocular drug delivery. However, the presence of surfactants can sometimes irritate tissues. Furthermore, conventional emulsions often have poor retention on ocular tissue. Pickering emulsions stabilised with nanoparticles have been gaining attention in recent years for a range of biomedical applications because of their biocompatibility. Here, Pickering emulsions were evaluated for the first time for the confinement of organic components for potential application in ocular drug delivery. For a model system, we used nanodiamond (ND) nanoparticles functionalised with covalently-bonded two-tail (2T) oligoglycine $C_{10}(NGly_4)_2$ to make Pickering oil-in-water emulsions, which were stable over three months of storage under neutral pH. We proved the non-toxicity of ND–2T Pickering emulsions, comparable to buffer solution, *via* an *ex vivo* bovine corneal permeability and opacity test. The retention of the oil phase in the ND–2T stabilised emulsions on corneal tissue is significantly increased because of the mucoadhesive properties arising from the positively-charged terminal amino groups of 2T. Our formulated emulsions have a surface tension, pH and salt concentration comparable to that of tear fluid. The high retention of the ND–2T-stabilised emulsions on the corneal surface, in combination with their non-toxicity, gives them distinct advantages for ocular drug delivery. The principles of this model system could be applied in the future design of a range of formulations for drug delivery.

Received 13th April 2023,
Accepted 3rd July 2023

DOI: 10.1039/d3sm00495c

rsc.li/soft-matter-journal

1. Introduction

Out of the 2.2 billion people in the world who have a visual impairment, approximately one billion could have been preventatively treated or are yet to be treated.[1,2] Ocular drug delivery formulations are required to address the problem of visual impairment. The purpose of such systems is to maintain therapeutic drug concentrations at the target site, minimise dosage frequency, and overcome various dynamic and static ocular barriers.[3] Although topically applied eye drops are used by clinicians to treat anterior segment disorders, such as dry eye disease, keratitis, and allergic conjunctivitis,[3] the relatively low drug bioavailability resulting from several factors is a major disadvantage. These factors include the continuous production of tear fluid and its drainage through the nasolacrimal duct to the nasal cavity, poor permeability of the cornea, and the removal of the drug by blinking.

To improve drug bioavailability, ophthalmic formulations require higher pre-corneal residence times and better drug penetration through ocular membranes. Therefore, drug delivery systems that provide longer retention times on ocular surfaces to facilitate the sustained release of drug molecules are required. Taking advantage of the negatively-charged glycocalyx covering the corneal surface,[4] the use of positively-charged particles or polymers is a common method for increasing the retention time of ocular formulations.[5] For example, a cationic polysaccharide, chitosan, and its derivatives are widely used for enhancing the mucoadhesive properties of various formulations.[6]

Oil-in-water emulsions are commonly used to formulate poorly water-soluble drugs for ocular drug delivery.[7,8] They are usually prepared as eye drops and emulsified using conventional or polymeric surfactants, such as poloxamers (*e.g.*, Poloxamer 188), polysorbates (*e.g.*, Tween 20), poly(ethylene glycol), Brij®, and tyloxapol.[9] Moreover, surfactants can improve

[a] *School of Mathematics and Physics, Faculty of Engineering and Physical Sciences, University of Surrey, Guildford, GU2 7XH, UK. E-mail: j.keddie@surrey.ac.uk*
[b] *Reading School of Pharmacy, University of Reading, Whiteknights, Reading, RG6 6DX, UK*
[c] *Physicochemical, Ex Vivo and Invertebrates Tests and Analysis Centre (PEVITAC), University of Reading, Whiteknights, Reading, RG6 6DX, UK*

† Electronic supplementary information (ESI) available. See DOI: https://doi.org/10.1039/d3sm00495c

drug permeation through the cornea.[10] For instance, Tween 20 was shown to be effective in increasing corneal permeability.[11]

Some classical surfactants widely used to stabilise emulsions, such as anionic sodium lauryl sulphate,[12] cationic cetylpyridinium chloride[13] or non-ionic polysorbates,[11] can cause tissue irritation or even damage to biological cells,[14,15] which limits their applications in ocular drug delivery. Pickering emulsions are particle-stabilised liquid droplets dispersed in an immiscible continuous liquid phase.[16,17] Compared to conventional surfactant-stabilised emulsions, Pickering emulsions can potentially show attractive qualities, including long-term stability against coalescence and the biocompatibility of the emulsifiers. Non-irritating nanoparticles used to stabilise Pickering emulsions could offer advantages in the formulation of ocular drug delivery systems. To the best of our knowledge, there are no prior reports in the literature on the use of ocular drops formulated as Pickering emulsions.

Pickering emulsions have previously been investigated for transdermal drug delivery. For example, Simovic and co-workers[18] studied the stability, structural and transdermal delivery characteristics of Pickering emulsions stabilized by hydrophilic biocompatible silica nanoparticles. They showed the importance of considering both delivery efficiency and potential toxicological risks. Accordingly, the selection of particles with biocompatible properties is very important for Pickering emulsions as drug delivery systems.

The biocompatibility, stability and facile surface modification of carbon-based particles make them an attractive choice as Pickering emulsion stabilisers.[19] Nanodiamond (ND) particles have been reported to exhibit better biocompatibility (and lower toxicity) compared to other carbon nanomaterials, such as carbon black, carbon nanotubes, carbon nanohorns, carbon nanoplatelets, and graphene oxide.[20–23] This conclusion was derived from a variety of methods, such as the MTT assay, mitochondrial membrane permeability (MMP) measurement, and reactive oxygen species (ROS) generation detection, utilizing neuronal and lung cell models by Schrand and coworkers.[24] Moreover, ND offers advantages in biomedical and pharmaceutical applications owing to a high loading capacity and an ability to cross cellular membranes.[25] Effective techniques for producing non-aggregated ND particles open new and exciting opportunities for applications in colloidal technology.[26] In addition, the functionalization of ND with carboxylic groups allows the covalent bonding or adsorption of molecules of interest in biomedicine, as well as demonstrating drug-loading capabilities.[27–29] Surface functionalization with carboxylic groups offers greater colloidal stability of ND when dispersed in polar solvents[30–32] as well as their enhanced biocompatibility, which is of great importance for their biomedical applications.[33]

In our previous work,[34] we demonstrated for the first time the feasibility of producing carboxylated ND-stabilised Pickering emulsions. However, the stability of these emulsions at neutral pH was found to be relatively low compared to emulsions with acidic or basic pH. Many ophthalmic solutions have an acidic pH range (3.5–6.3) that may cause discomfort upon initial application.[35] Therefore, extending the stability and lifetime of the ND-stabilised Pickering emulsions at neutral pH is one of our aims here.

Wettability is an important parameter of the nanoparticles that determines their suitability as Pickering emulsions. Raising the pH is a common approach to increase the wettability of carboxylated colloidal particles, but surface modification can offer considerable scope for designing multifunctional hybrid nanoparticles that can act as novel and efficient Pickering emulsion stabilisers.[36] For example, Zhao *et al.*[37] reported novel switchable silica nanoparticles modified by mixed polymer brushes of poly(acrylic acid) and polystyrene. Those functionalised particles can form stable dispersions in various solvents with the reorganization of polymer chains based on surrounding solvent conditions. Using the same mechanism, Motornov and coworkers[38] fabricated responsive nanoparticles by employing hybrid copolymer brushes and demonstrated a reversible switching between stable water-in-oil (w/o) and o/w emulsions. More recently, Yandrapalli *et al.*[39] used 3-allyloxy-2-hydroxy1-propane sulfonic acid to modify graphitic carbon nitride nanopowders, then produced monodispersed Pickering emulsions and demonstrated their potential applications in bioimaging, catalysis, and photonics.

Two-tail oligoglycine, $C_{10}(NGly_4)_2$ (referred to hereafter as 2T), consists of a middle alkyl chain between four glycine amino acid residues (tetrapeptides) at both ends of the molecule. 2T has been studied in depth, notably because of its special 2D self-assembled structure in neutral pH buffer solutions and its pH-responsive properties arising from its positively-charged terminal amino groups.[40,41] We have previously used self-assembled sheets of 2T to emulsify oil in water at a neutral pH.[42] We now hypothesise that the charged terminal amino groups on 2T will enhance mucoadhesion on ocular tissue. However, emulsions stabilised by 2T alone do not have adequate stability at a neutral pH for ocular drug delivery. Accordingly, we have developed a new type of model Pickering emulsion system stabilised by ND with covalently-bonded 2T, never reported previously. We used sunflower oil, which has been employed previously in eye drop applications,[43] as the oil phase in the Pickering emulsions. Using freshly excised bovine eyes as substrates, we investigated the toxicity of the composites and also explored the retention of the Pickering emulsions on the cornea. This model system will establish principles upon which to develop future ocular drug delivery formulations.

2. Results and discussions

2.1. Nanodiamond functionalisation and Pickering emulsification

2T was covalently bound to the surface of ND *via* a coupling reaction, which is schematically shown in Fig. 1. *N*-(3-Dimethylaminopropyl)-*N*′-ethyl carbodiimide hydrochloride (EDC) and *N*-hydroxysuccinimide (NHS) were used to mediate the reaction between the carboxylic groups on the ND surface and amino groups of 2T to form stable amide bonds.[44] This is the first example of this coupling reaction being applied to ND

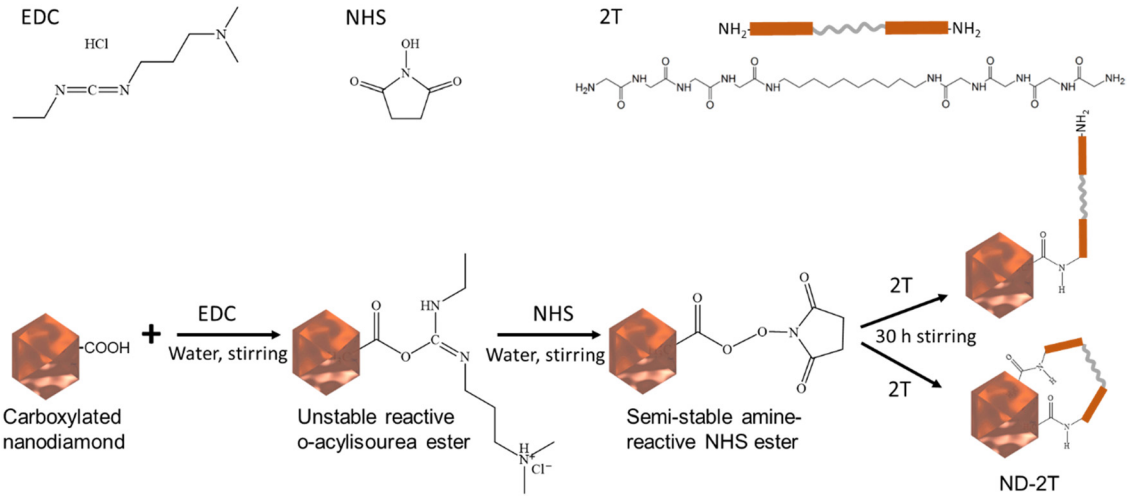

Fig. 1 The surface modification of ND particles with 2T. EDC and NHS produce a semi-stable amine-reactive ester on the ND surface. 2T replaces the ester and is covalently bonded to the ND surface.

and the first reported covalent grafting of 2T to ND. We refer to the functionalised nanoparticles as ND–2T.

Transmission electron microscopy (TEM) images of both ND and ND–2T are presented in Fig. 2. Individual ND particles, with a mean size of 4.8 ± 1.0 nm, are observed (Fig. 2a). The nanocrystals form aggregates following their drying from the water phase (pH = 7) during the TEM sample preparation. After undergoing surface modification of ND with the 2T, the morphology of the nanoparticles is significantly altered, as is presented in Fig. 2b. A large ND–2T cluster (*ca.* 100 nm in diameter) composed of modified nanoparticles (>20 nm) is visible. A coating layer on the ND nanoparticles (possibly grafted 2T) is observed in the inset image. The ND–2T particles might be formed by 2T being sandwiched between ND nanocrystals, with each end of the 2T molecules covalently binding to the facing ND crystals.

Evidence for the successful covalent bonding of the 2T to the ND *via* the EDC/NHS coupling reaction is provided by FT-IR spectra (Fig. 2c). Characteristic spectral bands at 1646 and 1560 cm^{-1} are assigned to the C=O stretching and N–H bending of 2T. The broad absorption band between 3700 cm^{-1} and 2700 cm^{-1} is assigned to the O–H stretching of carboxylic groups on the surface of ND particles. After the surface modification of ND with 2T, the relative intensity of the broad O–H stretching band in the ND spectrum is decreased. Additionally, the intensity of NH_2 wagging at 893 cm^{-1} in the 2T spectrum is greatly reduced in the ND functionalised with 2T following the conversion of some of the amino groups to amide bonds.

Thermogravimetric analysis (Fig. 2d) confirms that both 2T and ND are present in the nanoparticles functionalised with 2T (ND–2T). The first mass loss of 2T (56.5%), which is observed in the range from 200 °C to 400 °C, is explained by the defragmentation of linear peptides accompanied by the release of NH_3 and CO_2.[45] A mass loss is observed over the same temperature range for NDs functionalised with 2T where 28.4% of the mass is lost. As the mass loss of ND in this temperature range is 2.8%, then the mass percentage of 2T in ND–2T particles can be estimated as

$$m_{2T} \times 56.5\% = m_{ND-2T} \times 28.4\% - (m_{ND-2T} - m_{2T}) \times 2.8\%$$

where m_{2T} is the mass of 2T in ND–2T particles and m_{ND-2T} is the total mass of the ND–2T. Thus, we obtain $m_{2T} = 47.7\%\ m_{ND-2T}$, which is comparable to the initial proportion of reactants: 50% 2T by mass. According to the calculations presented in the ESI,† the surface coverage of 2T on ND is estimated from the mass analysis to be about 16 wt% of a dense 2T shell. The slightly higher decomposition temperature for the ND–2T, in comparison to the unmodified ND, can be explained by the amide bonds between 2T and ND. This difference provides additional evidence for the successful functionalization of NDs.

The ζ-potential and particle size of ND and ND–2T dispersions in water were evaluated over a wide range of pH (Fig. 2e) as a means to characterise the surface modification. The ζ-potential values for ND dispersions change from −20 mV to −31 mV upon increase in pH from 4.0 to 10.0, which is related to the deprotonation of the carboxylic groups. The changes of ζ-potential values for ND–2T particles are very different in the same range of pH. At pH 4.0 these particles are positively charged (ζ = +10 mV), because of the protonation of amino groups of 2T present on the ND surface. The zeta potential of 2T at pH 4 is +22.2 mV, which explains the switch from negative to positive charge after the ND was modified. A further increase in pH results in the recharging of the particles, and at pH 5.0, the ζ-potential has a negative value (−15 mV), owing to the presence of carboxylic groups on the ND surface, which were not substituted with 2T.[46] The isoelectric point (pH_{IEP}) is thus observed in the pH range between 4.0 and 5.0. At neutral pH, electropositive amino groups are present on the ND surface, despite the overall net negative charge. It is likely that some 2T molecules undergo the coupling reaction at both ends, but the increase in charge provides evidence for single-end bonding on the carboxy.

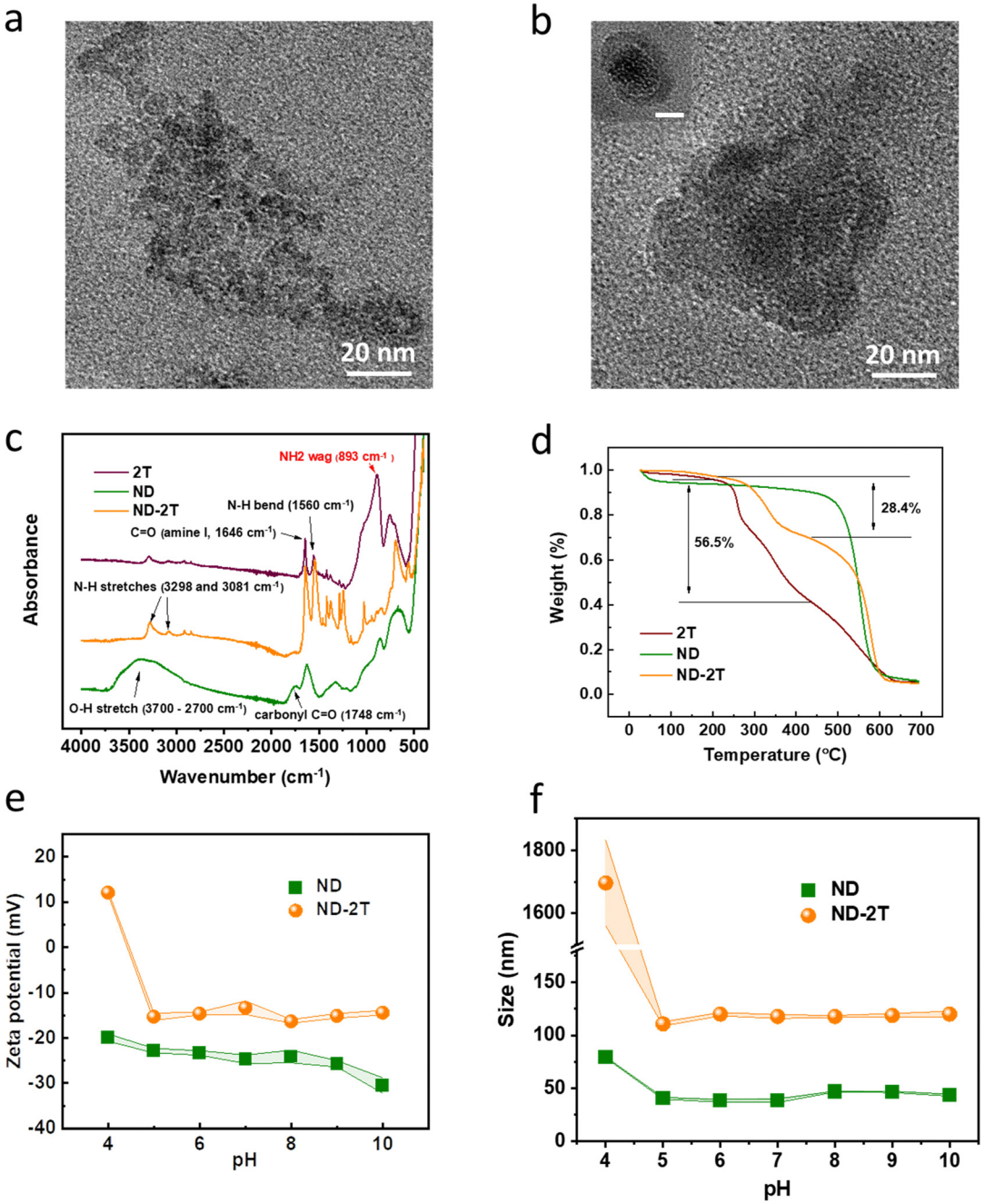

Fig. 2 Characterization of original ND and 2T-functionalised ND nanoparticles in water. TEM images of (a) ND and (b) ND–2T nanoparticles deposited from water (pH = 7). The scale bar in the inset is 20 nm. (c) FT-IR spectra of 2T, ND and ND–2T samples. (d) TGA thermograms of ND, 2T and ND–2T samples. (e) ζ-potential and (f) z-average particle size as a function of the pH value of ND and ND–2T particles. (Concentration in dispersions is 0.1 mg mL^{-1}). The upper and lower lines connecting the data points show the standard deviation.

The changes with the hydrodynamic diameter of ND and ND–2T particles, measured using dynamic light scattering, as a function of pH are shown in Fig. 2f. In agreement with the TEM analysis, the size of ND–2T particles is consistently higher than the original ND. At pH = 4.0, the unmodified ND exhibit a z-average particle size of 75 $\pm$ 1 nm; however, a further increase in pH $>$ 5.0 results in a substantial reduction of their diameter to 37 $\pm$ 1 nm. This is likely related to the deprotonation of carboxylic groups upon the increase in pH. At a more acidic pH of 4.0, the majority of carboxylic groups present on ND surface are protonated (pK_a approximately 4–5) and form interparticle hydrogen bonds causing their aggregation. When pH $>$ 5.0 the carboxylic groups are dissociated and cannot form hydrogen bonds, resulting in the de-aggregation of particles. The size of ND–2T is substantially larger than the diameter of unmodified ND at all pHs studied, even though the fully extended length of the 2T molecule is only 4 nm. This could be related to the possibility that some 2T molecules could have

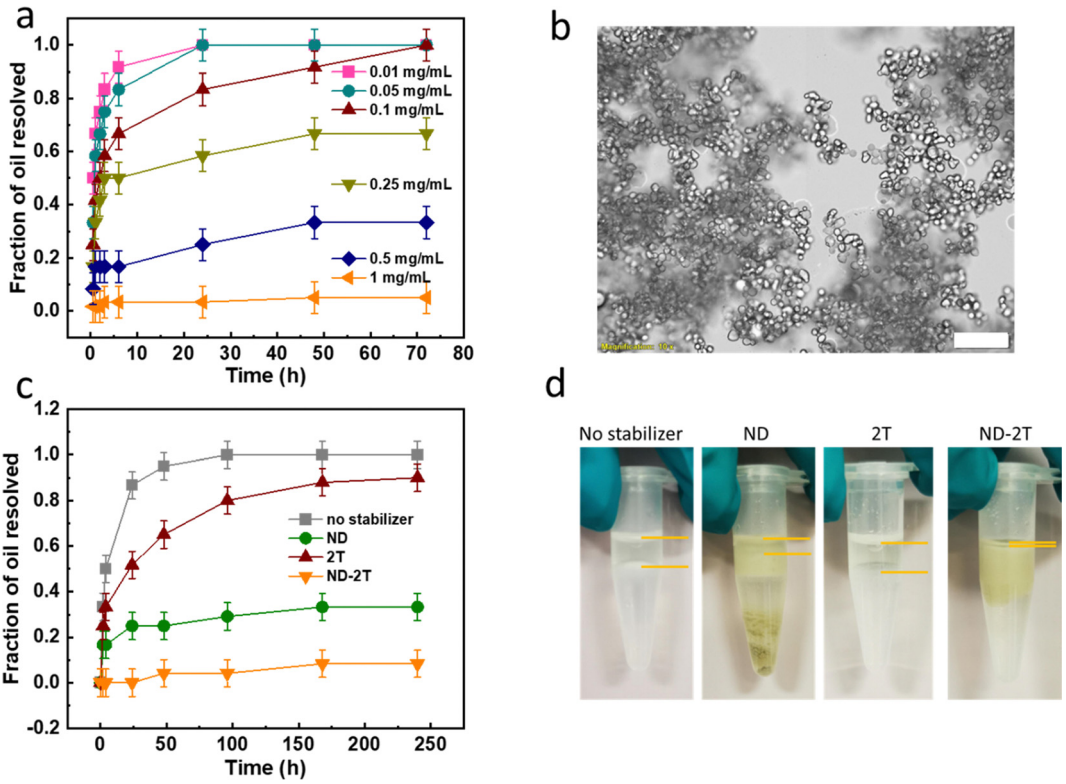

Fig. 3 (a) Time dependence of the destabilization of ND–2T stabilised Pickering emulsions (measured by the thickness of free oil layer) at different particle concentrations. (b) Optical microscopy image of 1 mg mL^{-1} ND–2T-stabilised Pickering emulsion at 0.5 h after their formation. The scale bar represents 100 μm. (c) Comparison of the destabilization of four emulsions with either no emulsifier or with three different Pickering stabilisers: 1 mg mL^{-1} ND, 1 mg mL^{-1} 2T, and 1 mg mL^{-1} ND–2T. (d) Digital photographs of the four different emulsions after being stored in the dark for three months.

reacted from both ends and linked several particles together covalently, as was also suggested by the TEM analysis. The largest particle size for ND–2T is observed at pH 4.0 (>1000 nm), indicating strong aggregation. This result could be related to the proximity of this pH to the pH_{IEP} where number of positively charged groups equals the number of negatively charged groups. This sort of aggregation behaviour is well documented in some synthetic and natural polyampholytes, which tend to aggregate and precipitate at pH = pH_{IEP}.[47,48] When the pH > 5.0 the particles gain negative charge and attain a stable diameter of 110 ± 2 nm.

Chemical modification of ND with organic molecules to strengthen their fluorescent properties has attracted great attention in recent years owing to their potential applications in theranostics.[49,50] In the present work, we have studied the fluorescence of the ND–2T particles as a means to characterise the chemical modification of the ND (ESI† Fig. S1). At the excitation wavelength of 460 nm, a fluorescent peak at 521 nm is observed for ND. For the ND–2T particles, a new peak at 580 nm is observed, which might be arising from the non-diamond carbon (amorphous and not chemically pure) on the ND particle surface.[51]

Having synthesised ND–2T particles and determined their fundamental properties, we developed their use in Pickering emulsions. A range of concentrations of ND–2T in deionised water dispersions (0.01 mg mL^{-1}, 0.05 mg mL^{-1}, 0.1 mg mL^{-1}, 0.25 mg mL^{-1}, 0.5 mg mL^{-1} and 1 mg mL^{-1}) was prepared for the emulsification of sunflower oil with a water : oil volume ratio of 7 : 3. The emulsion stability was determined by measuring the volume fraction of de-emulsified oil over time. As is shown in Fig. 3a, when the ND–2T particles concentration was increased, the stability was improved at the same time. When the ND–2T concentration was increased to 1 mg mL^{-1}, barely any oil layer was observed over 72 h of ageing, indicating the formation of stable ND–2T Pickering emulsions. Fig. 3b shows a microscopy image of the 1 mg mL^{-1} ND–2T stabilised emulsions at 0.5 h after their formation, which gives a mean size of 16 μm and a coefficient variation of 18%.

Emulsions prepared with three different stabilisers (1 mg mL^{-1} ND, 1 mg mL^{-1} 2T, and 1 mg mL^{-1} ND–2T) with the same formulation (with a water : oil volume ratio of 7 : 3) are compared in Fig. 3c. There is an obvious improvement in the stability of emulsions prepared in the presence of ND–2T compared to ND and 2T over 240 h of their storage. Even after three months of storage (Fig. 3d), almost no phase separated oil was observed, although the size of oil droplets was doubled (Fig. S2 in ESI†) which can be attributed to some coalescence. With 2T used as an emulsifier and without any added emulsifier, the emulsions started to destabilise over the first few hours and were nearly fully destabilised after 240 h. Distinct oil layers were found in these formulations after three months of their storage. In the emulsions stabilised with ND, about one half of

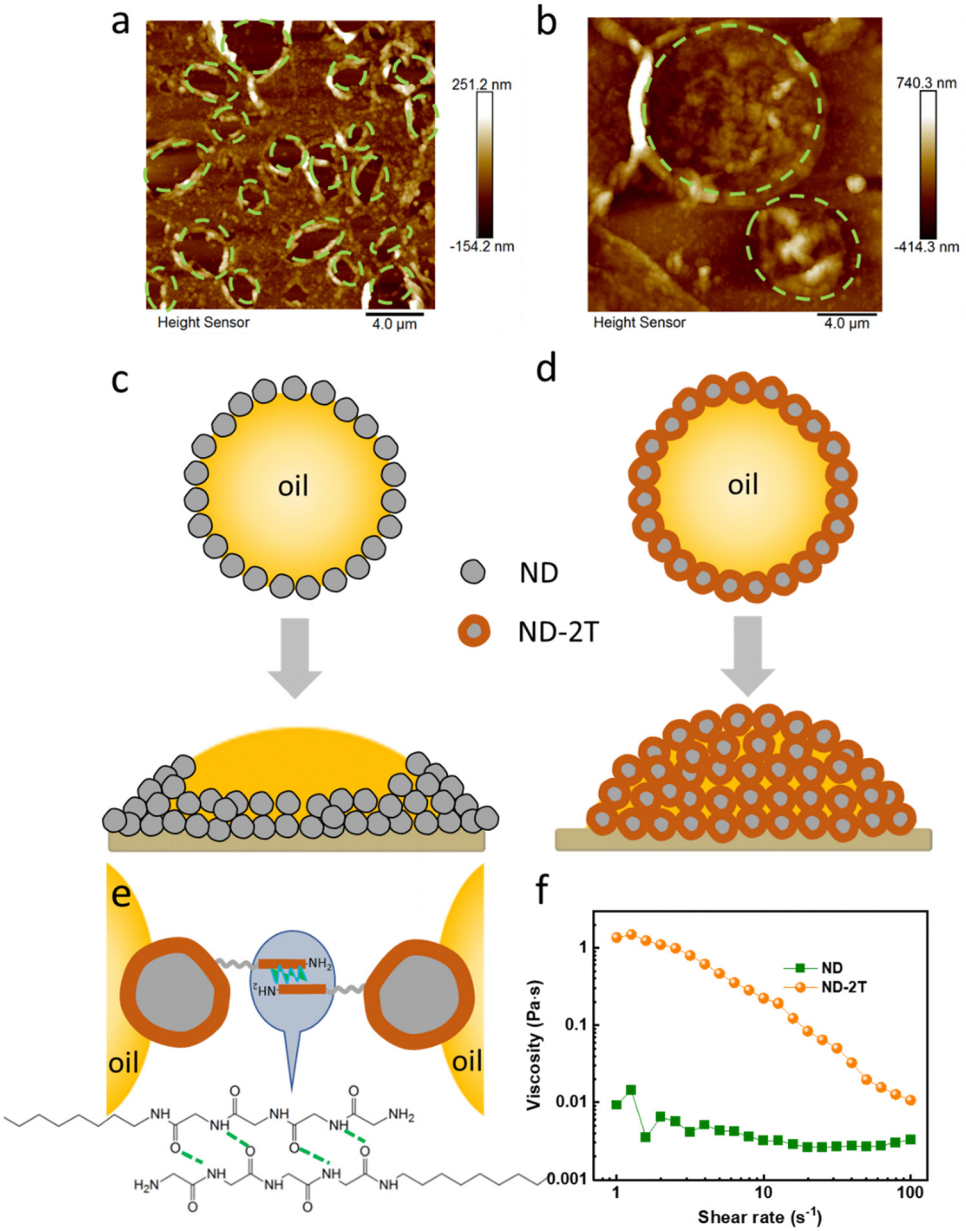

Fig. 4 (a) AFM images of a dried ND emulsion film on a glass substrate. (b) AFM images of dried ND–2T emulsion film on glass. In (a) and (b), the oil phase was removed *via* immersion in toluene. Schematic diagrams show an interpretation of inter-particle interactions for (c) an ND-stabilised oil drop and (d) an ND–2T-stabilised oil drop. The top drawings show a cross-sectional view of the Pickering emulsion oil drops. The bottom drawings show the result after depositing onto a solid substrate and removing the water phase. (e) The possible H-bonding between the oligoglycine segments on adjacent 2T–ND particles. (f) Viscosity for the Pickering emulsions stabilised with ND and ND–2T as a function of shear rate.

the volume remained after three months, and sedimentation of ND was observed, which is attributed to the de-emulsification resulting in the formation of precipitates at the bottom of the container. The stability improvement of emulsions stabilised with ND–2T, compared to ND, is in good agreement with previous reports that a lower absolute value of ζ-potential of particles tends to impart a Pickering emulsion with higher stability,[52–54] while less charged particles have lower polarity and therefore greater affinity for the oil/water interface. Note in Fig. 2e that ND–2T particles have a ∼10 mV lower negative ζ-potential compared to ND dispersions at pH 7.

Additional experiments to explore the stabilization mechanism of ND–2T emulsions were performed. Emulsions stabilised with either ND or ND–2T were diluted and dried on a glass substrate. The stabilised emulsion drops were then immersed in toluene to remove the oil phase to allow imaging of the stabilising shells *via* atomic force microscopy (AFM). Fig. 4a shows the AFM images of an ND-stabilised emulsion film, in which there is an ND coating with many open holes (highlighted by the green dashed circles), which otherwise would be the position of the oil droplets before being removed. At the edge of the open holes, the ND density is higher than in other

areas. In contrast, for the dried ND–2T-stabilised emulsion film (with oil removed), no such holes are found (Fig. 4b). Instead, there are hemispherical structures which are interpreted as the remains of the ND–2T shells that previously encapsulated the oil droplets. In the microscope images in Fig. S3 (ESI†), more evidence for hemispherical "oil drops" is found in the dried ND–2T emulsion. Based on these observations, we present a schematic diagram to illustrate the proposed stabilization mechanisms (Fig. 4c and d). For the ND-stabilised oil droplets, because of the weak particle interactions between the ND particles at the oil surface, the ND particles migrate to the edge of the oil droplet under gravity during the drying of the emulsion. However, for the ND–2T stabilised oil droplets, adhesion between ND–2T nanoparticles results from the hydrogen bonding between the tetrapeptide segments (N–H···O) on adjacent nanoparticle surfaces (Fig. 4e). Gravitational forces on the particles cannot overcome these H-bonding attractions, and therefore a hollow capsule is formed upon the oil removal. This type of capsule will increase the ND–2T emulsion stability.

This interpretation is supported by the rheological analysis shown in Fig. 4f. The ND–2T stabilised emulsions show a typical shear-thinning behaviour, wherein the viscosity decreases as the shear rate increases, until it reaches the same level as the viscosity of the ND-stabilised emulsions. The shear-thinning behaviour can be explained by decreasing interactions between ND–2T particles on contacting oil drop surfaces, when hydrogen bonds are disrupted by the shearing force.[55] In contrast, for the ND-stabilised emulsions, without hydrogen bonding between emulsion droplets, the viscosity remains at a constant value during shearing, which agrees with previous rheological studies by Farias *et al.*[56] using hydroxylated ND as a Pickering emulsion stabiliser.

2.2. Evaluation for ocular drug delivery applications

Any formulation designed for topical administration to the eye should meet a range of requirements. One of these is absence of adverse effects on the ocular surface. For example, the pH of the formulation should be close to the normal pH of tear fluid (in the pH range between 7.14 and 7.82) to reduce discomfort and to minimise lacrimation.[57] In the present work, we prepared the ND–2T stabilised emulsion using DI-water, and the pH was measured to be 7. The osmotic pressure of tears is equivalent to a 0.9% to 1.0 wt% solution of sodium chloride. Hypotonic and hypertonic solutions are problematic. To explore the feasibility of the Pickering emulsions for ocular delivery, sodium chloride was added to the aqueous phase of an ND–2T emulsion to make a 1 wt% solution. The emulsion remained stable after the salt addition, and the size of the oil drops did not change during one day of observation. Additionally, the surface tension value of normal tear fluid from healthy human eyes[58] falls in the range of 43.6 ± 2.7 mN m^{-1}. Solutions with a surface tension lower than that of tears may disrupt the lipid layer of the tear film, causing it to form lipid droplets. The integrity of this oily film, created by the lacrimal fluid, is crucial for maintaining a healthy tear film by keeping the eye hydrated and preventing dry eye.[59,60] In this work, the surface tensions of three emulsions (Tween-20, ND and ND–2T stabilised) were measured *via* pendant drop tensiometry (Fig. S4 in ESI†). The values for all three emulsions fell within the range of the surface tension of tear fluid. The ND–2T-stabilised emulsion has an acceptable surface tension of *ca.* 46 mN m^{-1}, which can be attributed to the presence of excess ND–2T particles or emulsion oil droplets adsorbing at the air–water interface.

The bovine corneal permeability and opacity (BCOP) assay has been commonly used to evaluate the biocompatibility of ocular formulations, specifically for the identification of corrosive and severe ocular irritants.[61,62] BCOP typically consists of two separate tests, involving (a) the effect of chemicals on the opacification of the bovine cornea, and (b) their effect on the integrity and barrier function of the corneal epithelium. The barrier function of the corneal epithelium is assessed *via*

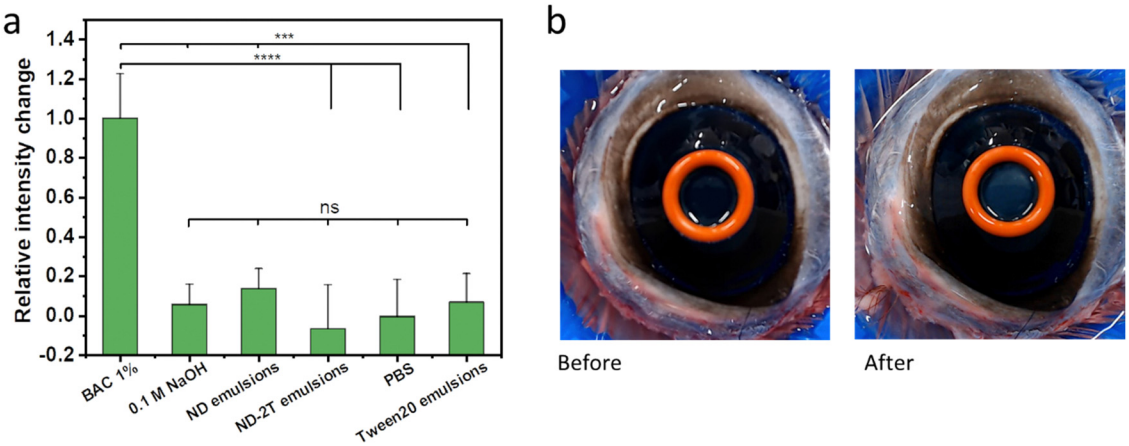

Fig. 5 (a) Changes in bovine corneal opacity following their exposure to 1% w/v BAC, 0.1 M NaOH, 1 mg mL^{-1} ND-stabilised emulsion, 1 mg mL^{-1} ND–2T-stabilised emulsions, PBS buffer (pH 7.4), and 1 mg mL^{-1} Tween 20-stabilised emulsions. The values are presented as the difference in the mean intensity ± standard deviation (n = 3) relative to the blank tissue, then normalised by the highest intensity difference (obtained for BAC 1%). Statistically significant differences are represented as: **** $p < 0.0001$; *** $p < 0.001$; ns (no significant difference) $p \geq 0.05$. (b) Digital *p*hotographs showing a bovine eye before and after it was treated with 1% w/v BAC. The orange silicone ring encircles the cornea where the BAC was added.

the permeation of sodium fluorescein following the tissue exposure to a test chemical.

In this research, BCOP was used for the preliminary screening of emulsions stabilised using ND, ND–2T and Tween 20. Their results are compared to those of benzalkonium chloride (BAC), which is commonly present at a concentration of 0.02% w/v in approximately 70% of commercial ophthalmic formulations as a preservative and penetration enhancer. However, at higher concentrations (*e.g.* 1% w/v), it causes severe ocular irritation.[63] A 0.1 M NaOH solution was used as a positive control because this base is known to be corrosive to corneal tissue at high concentrations.[64] PBS buffer (pH 7.4) and a conventional emulsion made using Tween 20 (1 mg mL^{-1}) were both negative controls. Tween 20 is a surfactant that has been commonly used in ocular formulations.[65] Pickering emulsions stabilised by 2T alone are poorly stable at neutral pH.[42] Hence, they are considered unsuitable candidates for ocular drug delivery and were not studied here.

Results of the corneal opacity experiments are presented in Fig. 5a. The data show that 1% w/v BAC significantly changed the opacity of the bovine cornea ($p < 0.05$), confirming its strongly irritant nature at this concentration. Effects can even be observed visually (Fig. 5b). The exposure of the bovine cornea to PBS caused no significant changes in the corneal opacity ($p > 0.05$). Similar results were found for 0.1 M NaOH and the three emulsions. There were no statistically significant differences in the opacity changes observed for the exposure of bovine cornea to the emulsions

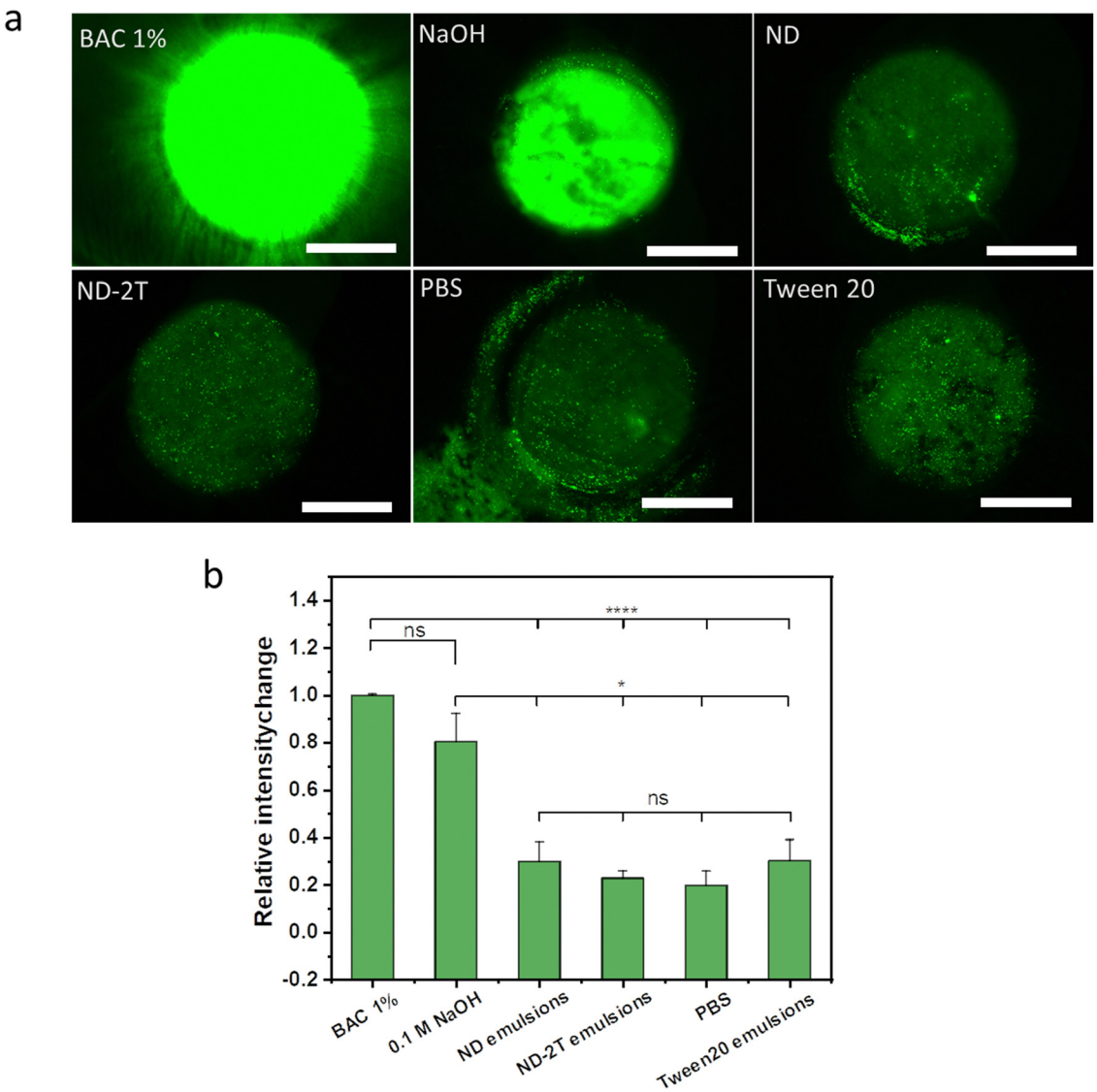

Fig. 6 (a) Fluorescent images of bovine eyes treated with sodium fluorescein following their exposure to 1% w/v BAC, 0.1 M NaOH, PBS buffer (pH 7.4), and o/w emulsions stabilised with 1 mg mL^{-1} ND, 1 mg mL^{-1} ND–2T, and 1 mg mL^{-1} Tween 20. The scale bar represents a length of 4 mm. (b) Change in fluorescent intensity values after the application of test substance (normalised by the intensity change for BAC 1%). Intensity values were calculated from raw images using ImageJ software. The values are presented as mean ± standard deviation ($n = 3$). Statistically significant differences were represented as: **** $p < 0.0001$; * $p < 0.05$; ns (no significant difference) $p \geq 0.05$.

stabilised with ND, ND–2T, and Tween 20 compared to the PBS buffer.

The cornea protects the eyes from the penetration of hazardous substances[66,67] and its barrier function can be evaluated using sodium fluorescein.[61] Damage to the cornea by exposure to irritant compounds results in epithelial disruption, making it more permeable to the fluorescent molecule. Fig. 6a shows exemplar fluorescent images of bovine corneas pre-treated with 1% w/v BAC, 0.1 M NaOH, the three emulsions, and PBS, and subsequently exposed to sodium fluorescein solution. The normalized relative fluorescent intensity values, in Fig. 6b, provide a comparison of the effects of these compounds and formulations on the corneal permeability to sodium fluorescein. Relatively high fluorescent intensity values recorded for the exposure of bovine corneas to 1% w/v BAC and 0.1 M NaOH indicate that these compounds cause disruption in the barrier function of the epithelia. The PBS buffer-treated cornea shows the lowest fluorescent intensity which implies no corneal damage. There are no significant differences in the fluorescent intensity between the PBS-treated corneas and the corneas treated with ND, ND–2T-, and Tween 20-stabilised emulsions, which means there is no corneal damage from these formulations. Overall, the results of BCOP assay indicate that emulsions stabilised with ND and ND–2T should cause no ocular irritation if eventually used in drug delivery.

Conventional eye drops are often characterised by relatively poor retention on the ocular surfaces because of continuous tear production, blinking, and nasolacrimal drainage. These factors – combined with the low permeability of the cornea – contribute to there being insufficiently low drug bioavailability when using eye drops.[68,69] The development of eye drops with greater retention on ocular surfaces will facilitate drug delivery. Therefore, experiments to study ocular retention were conducted.

To evaluate the effectiveness as a vehicle for ocular drug delivery, the retention of the Pickering emulsions on the corneal surfaces was assessed using a fluorescence-based flow-through assay.[70,71] The oil phase was labelled with Nile Red dye to allow its easy visualization. Fig. 7(a–c) shows the fluorescence images of

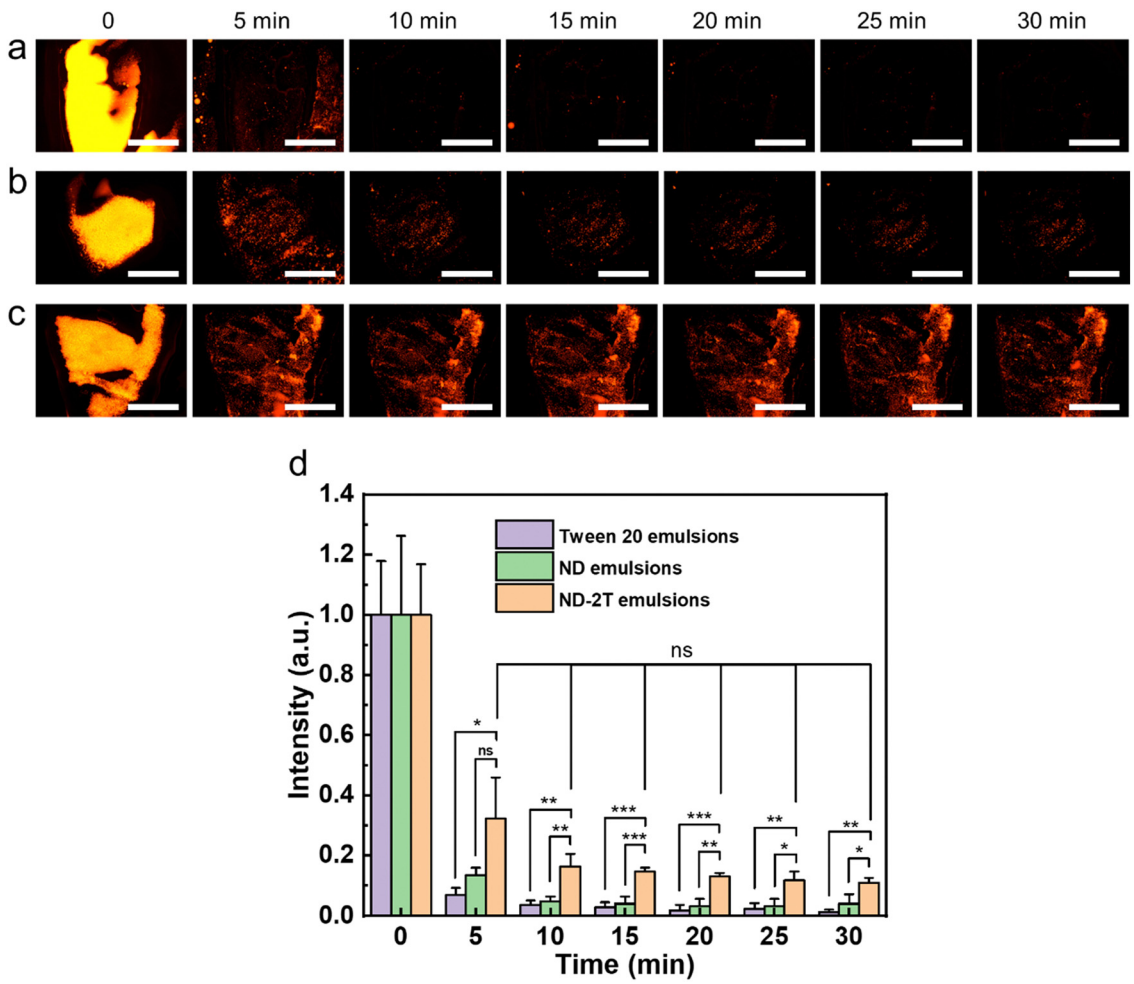

Fig. 7 Representative fluorescent images of bovine corneas with applied (a) Tween 20 emulsions, (b) ND-stabilised emulsions, and (c) ND–2T-stabilised emulsions during rinsing with SFT for 30 min. The oil phase contains Nile Red. The brightness and contrast of the images shown here were auto-adjusted for clarity. The scale bar represents 5 mm in all images. (d) Normalized relative fluorescent intensity values calculated from the raw images. The values are presented as mean ± standard deviation (n = 3). Statistically significant differences were represented as: *** $p < 0.001$; ** $p < 0.01$; * $p < 0.05$; ns (no significant difference) $p \geq 0.05$.

the Tween 20, ND, and ND–2T emulsions on the bovine corneas after rinsing with simulated tear fluid (STF) continuously over time. The normalized relative fluorescence intensity values were calculated from these images and are presented in Fig. 7d. The data show that Tween 20 emulsions nearly fully rinse off from the cornea in less than 10 min, and only a small amount (1.3 ± 0.7%) of oil remains after 30 min. Only 4.0 ± 3.1% of the oil in the ND-stabilised emulsion remains on the cornea after 30 min of rinsing with STF. However, the ND–2T stabilised emulsion demonstrates superior retention on the bovine cornea (Fig. 7) with 11.0 ± 1.7% of the oil formulation remaining on the mucosal surface of the cornea after 30 min of STF rinsing. This greater retention of the ND–2T stabilised Pickering emulsion is likely arising from mucoadhesion between the negatively-charged glycocalyx of the cornea[4] and the positively-charged amino groups of 2T on the ND at the oil droplet surfaces. The oil stabilised by negatively-charged ND is not retained as well without this mechanism of mucoadhesion.

3. Conclusions

Nanodiamond particles were modified with a two-tailed oligoglycine for stabilization of Pickering oil-in-water emulsions as a model system for potential applications in ocular drug delivery. These ND–2T Pickering emulsions remained highly stable for up to three months. These emulsions offer distinct advantages over conventional surfactant emulsions for ocular drug delivery. When applied to bovine eyes, there is no evidence that the ND–2T emulsions damage the cornea from BCOP and fluorescein penetration tests. The functionalised ND does not pose any toxicity according to these tests. A distinct advantage of the ND–2T Pickering emulsions is their mucoadhesion in comparison to conventional Tween 20 emulsions and ND-stabilised emulsions. Whereas the oil in the ND–2T emulsions is retained on the corneal surface with up to 30 min of rinsing, Tween 20 emulsions show very little oil retention after only 5 min. The retention by the Pickering emulsion is attributed to the charged terminal amino groups of the 2T corona on the ND particles, which provide electrostatic attraction to the mucins on the corneal tissue. The formulated ND–2T Pickering emulsions meet the requirements of eyedrops: a neutral pH, stable with 1 wt% NaCl in the aqueous phase, and a surface tension of 46 mN m^{-1}. Their low toxicity and irritation to tissue in combination with their higher retention give the ND–2T Pickering emulsions distinct advantages in ocular drug delivery.

In future work, the concepts of this model Pickering emulsion could be applied in the formulation of drug delivery systems for the cornea and other mucosal tissues. A range of other types of modified nanoparticles could be used as Pickering stabilisers as a replacement for surfactants. A key insight is that functionalisation of the nanoparticles with electropositive molecules increases retention through mucoadhesion, even when the particle carries a net negative charge. Future research should investigate the penetration of the ND–2T nanoparticles and drugs into the cornea and the clearance of any non-adhering nanoparticles.

4. Materials and methods

4.1. Materials

Oligoglycine Gly_4–NH–$C_{10}H_{20}$–NH–Gly_4 (2T, purity > 95%) was purchased from PlasmaChem GmbH (Berlin, Germany) and used as received. Monodispersed, single-digit, carboxylated detonation ND (nominally 5 nm diameter, with a concentration of 10 mg mL^{-1} in water), *N*-(3-dimethylaminopropyl)-*N*′-ethyl carbodiimide hydrochloride (EDC, 99%), N-hydroxysuccinimide (NHS, 98%), benzalkonium chloride (BAC), and Nile Red (for microscopy in retention tests) were used as received from Sigma-Aldrich (Merck Life Science UK Limited; Gillingham, UK). Pure sunflower oil (Flora©, Princes Ltd, UK) was used as the oil phase (without any purification) to prepare o/w emulsions. Polyethylene glycol sorbitan monolaurate (Tween 20, product number P1379, Sigma-Aldrich) was used in comparative emulsions as a surfactant. Sodium chloride, sodium bicarbonate, calcium chloride dihydrate, and phosphate-buffered saline (PBS) tablets were purchased from Fisher Scientific UK Ltd (Loughborough, United Kingdom). Aqueous solutions of HCl and NaOH (0.1 M, purchased from Sigma-Aldrich) and deionised (DI) water (18.2 MΩ cm, Elga DI water system) were used in experiments.

4.2. Synthesis of ND–2T composites

The synthesis partly followed the method reported in the literature[72] to modify ND to graft it to hydroxylated surfaces through a silane coupling. Firstly, 2.5 mL of ND dispersions were added into a 20 mL vial and were diluted to 2.5 mg mL^{-1} by adding 7.5 mL DI water. Then 250 mg EDC was added with continuous stirring for 20 min while the pH was adjusted to *ca.* 5 with the addition of 0.1 M HCl. Afterwards, 300 mg of NHS (with the molar ratio of EDC : NHS calculated to be 1 : 2) was added into the dispersion and stirred for 2 h to allow the activation of the ND. Then, 25 mg 2T was added to the mixture, and the pH was adjusted to *ca.* 7 by adding 0.1 M NaOH. After 30 h of stirring, the product was transferred to a centrifuge tube for purification. DI water, pH 4 HCl solutions, and pH 10 NaOH solutions were used to purify the product by sonication and centrifuged for 10 min at 4000 rpm separately. This purification was repeated three times for each solution. The final purified product was redispersed in DI water (2 mg mL^{-1}).

4.3. Preparation of ND–2T stabilised Pickering emulsions

Emulsification was achieved by probe sonication using a probe sonifier (Branson Sonifier 150). 700 μL ND–2T dispersions (or Tween 20 solutions or ND dispersions), and 300 μL of sunflower oil were added to a 2 mL Eppendorf tube. Then probe sonication with a power of 6 W and a sonication time of 15 s was used to prepare the Pickering emulsions.

4.4. Emulsion characterisation

4.4.1. Fourier transform-infrared spectroscopy. Fourier transform-infrared (FT-IR) spectra were recorded on a Perkin-Elmer Spectrum Two spectrometer equipped with an attenuated total reflectance (ATR) accessory by scanning in the 4000–500 cm^{-1} range with a resolution of 4 cm^{-1}. For the sample preparation,

the ND–2T dispersion and ND dispersion were dried at 100 °C on clean glass substrates on a hotplate to obtain solid powders. The dried powders were spread at the central part of the ATR accessory.

4.4.2. Thermogravimetric analysis (TGA). The thermal stability of ND, 2T and ND–2T composites was evaluated by employing thermogravimetric analysis (Discovery TGA 550, TA Instruments; New Castle, USA) in the temperature range from 26 °C to 700 °C in air with a heating rate of 10 °C min^{-1}.

4.4.3. Size and ζ-potential of ND dispersions. Dynamic light scattering (DLS) and ζ-potential measurements of the ND dispersions and ND–2T composite dispersions (from pH 4 to pH 10) were performed using a Malvern Zetasizer (Malvern Panalytical; Malvern, UK) at an optimal temperature (25 °C). The instrument was fitted with a 4 mW 632.8 nm He–Ne red laser and a detector (avalanche photodiode) positioned at 173° to measure the scattered light. All the dispersions were diluted (to about 0.1 mg mL^{-1}) until a single peak and well-fitted results were obtained. Reported values of particle size are *z*-averages from three independent measurements, and each measurement consisted of 12 runs.

4.4.4. Fluorescent characterisation of ND–2T composites. A microplate reader (BMG LABTECH, Germany) was used to monitor the fluorescence intensity of the ND before and after surface modification with 2T. The ND dispersions and ND–2T dispersions were diluted to *ca.* 0.8 mg mL^{-1} and sonicated before the measurement. The excitation wavelength was set to 460 nm, and the excitation wavelength between 480 nm to 600 nm was recorded.

4.4.5. Long-term emulsion stability. All emulsions produced by probe sonication membrane emulsification were stored at room temperature after they were produced. The fraction of oil resolved over time[73] was used to compare the stability (Fig. S5 in ESI†).

4.4.6. Morphological observations. The microstructures of the ND–2T Pickering emulsions were observed with an optical microscope (Olympus BX53M), equipped with 10×, 20×, and 50× objective lenses. The samples were prepared by placing several drops of emulsion on clean glass slides. Three images were analysed and 30 oil drops were randomly chosen from each of the images with ImageJ software (version 1.52n, 2019) to find the distribution of droplet sizes and the coefficient of variation.[74] Diameters of the oil droplets were determined from the areas of each droplet image, and mean values are reported hereafter to represent the droplet size.

The Thermo Scientific™ Talos F200i (S) TEM was used to measure the morphological structure of ND and ND–2T in water samples. All samples were diluted to 0.1 mg mL^{-1} and sonicated before casting them on a copper grid with carbon films cleaned with glow discharge. Digital images were analysed using the Analyse Particle function with Image J software to find ND particle mean size and standard deviation. 30 particles were randomly selected and analyzed.

AFM (Dimension Edge™, Bruker) was used to characterise the morphology of ND and ND–2T coatings from their dried emulsions. To prepare these samples, the same volume of ND emulsions and ND–2T emulsions were diluted 50 times and then dropped on a glass slide separately and dried at room temperature for two days to remove the water. The deposited coatings were then immersed in toluene for 10 min to remove the oil phase. After the toluene was evaporated, the coatings were imaged *via* AFM.

4.4.7. Rheological studies. The rheological properties of Pickering emulsions stabilised by ND and ND–2T nanoparticles were determined from 0.8 mL of each emulsion at ambient temperature (25 ± 0.01 °C) using an HR 2 Discovery rheometer (TA Instruments, New Castle, DE, USA). A stainless steel parallel plate geometry (40 mm diameter) with a sand-blasted stainless steel base plate set at a gap height of 1 mm was used. The apparent viscosity of the emulsions was measured over a range of shear rates from 1 to 100 s^{-1}.

4.5. *In vitro* tests of the emulsions on bovine eyes

4.5.1. Bovine corneal permeability and opacity test. The toxicity assessments of the emulsions were performed using the bovine corneal opacity and permeability (BCOP) test according to Abdelkader *et al.*[61] and Schrage *et al.*'s protocol,[62] with minor modification. Tests were performed on six different samples: PBS buffer (pH 7.4), NaOH (0.1 M), BAC (1% w/v), and o/w emulsions stabilised with either 1 mg mL^{-1} ND, 1 mg mL^{-1} ND–2T, or 1 mg mL^{-1} Tween 20.

Intact bovine eyeballs, provided by P.C. Turner Abattoirs (Farnborough, UK) after animal slaughter, were packed and transported in insulated bags with ice packs. All eyes were used within 12 h after slaughter. The freshly dissected eyeballs with the corneas facing upwards were wrapped with cling film and placed in plastic cups. Before each experiment, the microscope image of the blank tissue (*i.e.* original, as-received eyeball without test substance) was taken to measure the pixel intensity of the blank tissue to take any intrinsic fluorescence into account. For each eye, several drops of PBS solution were applied every 5 min to keep the eyes wet. The plastic cups were incubated in a water bath at 34 ± 1 °C for 10 min. A silicone O-ring (8 mm diameter) was placed on top of the cornea, as shown in Fig. S6a (ESI†). The eye was photographed with the silicone ring still in place using a digital camera (Logitech HD Pro Webcam C920). 0.1 mL of various test compounds (0.01 M NaOH, PBS, 1% w/v BAC, Tween 20 emulsions, ND emulsions, ND–2T emulsions) were then applied within the silicone ring separately. After 60 s of treatment, 10 mL of PBS solution was poured over to rinse off the test substances. Afterwards, the cup was left in a water bath for another 10 min at 34 ± 1 °C. In the next step, it was removed from the bath, the eye was photographed with the silicone ring using the camera again. And then 0.1 mL of 20 mg mL^{-1} sodium fluorescein solution was added to the ring and left for 60 s. The sodium fluorescein was rinsed off with 10 mL of PBS solution after ring removal. Then 1 mL PBS buffer was added drop by drop under the microscope to confirm that the excessive sodium fluorescein was removed. Following that, the fluorescence images of eyeballs were acquired using a Leica MZ10F stereomicroscope (Leica Microsystems, Wetzlar, Germany) with a GFP filter fitted with a Leica DFC3000G

digital camera at 1.25× magnification, 320 ms exposure time (gain 2×) at the intensity of 4. The emission wavelength was set as 512 nm.

The general procedures of the experiment are shown in Fig. S6b (ESI†). All fluorescence images were analysed using ImageJ software. To account for any background fluorescence, a fluorescence image of blank ocular tissue was obtained and subtracted from the test image when calculating the mean fluorescence intensity. The BCOP tests were conducted in three replicates for each formulation.

4.5.2. Mucoadhesive retention testing *via* a flow-through assay. The retention properties were assessed by a mucoadhesion test following our previous protocol with minor modifications.[75,76] Tests were conducted on three samples: ND stabilised emulsions, ND–2T emulsions, and Tween 20 emulsions. To allow measurement of the oil phase adhering to the cornea, it was labelled with Nile Red. This dye was mixed into the oil (0.5 mg mL^{-1}) prior to emulsification *via* probe sonication.

Simulated tear fluid (STF) was prepared according to the protocol described by Srividya *et al.*[77] 0.670 g of sodium chloride, 0.200 g of sodium bicarbonate, and 0.008 g of calcium chloride dihydrate were dissolved in 100 mL of deionised water at room temperature. The pH of the simulated tear fluid solution was adjusted to 7.4 by adding 0.1 M NaOH because the pH of natural tear fluid is close to neutral. The simulated tear fluid was kept at 34.5 °C in a water bath during the mucoadhesion tests.

The corneas were carefully excised with a scalpel within 3 h of delivery to the laboratory. Then these dissected corneas were rinsed with 1 mL of freshly prepared STF and mounted on glass slides with the outer epithelial layer facing upward. Before the mucoadhesion tests, the incubator was set at 34.5 °C. Then 20 μL of emulsions with Nile Red dye were applied to the center of the corneal surface as shown in Fig. S7a (ESI†). After 2 min, the cornea was irrigated with STF using a 60 mL syringe on a pump (Harvard Apparatus model 981074, Holliston, USA) at a flow rate of 100 μL min^{-1} for a duration of 30 min. This flow rate was selected to represent the normal tear production in human eyes, which is 1–2 μL min^{-1}.[57] The distance between the corneal surface and the syringe needle was fixed at about 1 cm. The inclination angle of the glass slide was 20°. A schematic diagram showing the experimental apparatus is given in Fig. S7b (ESI†).

Fluorescence images of cornea were acquired using a Leica MZ10F stereomicroscope (Leica Microsystems, Wetzlar, Germany) with a GFP filter fitted to a Leica DFC3000G digital camera at 1.25× magnification with a 907 ms exposure time (gain 2×) at an intensity of 4. The emission wavelength was set at 628 nm. The acquired microscopy images were then analysed using ImageJ software (version 1.52n, 2019) with the mean fluorescence values measured (after each irrigation with 0.5 mL of STF) with the subsequent calculation of the fluorescence intensity (%) for each time point where the initial point was set at 100%. Before each wash-off experiment, the image of the tissue (cornea without test substances) was taken to measure the blank tissue's pixel intensity for data normalisation. A histogram of the distribution of these fluorescence intensity values at different wash time points (0 to 30 min with increments of 5 min) was obtained as a function of time. All mucoadhesion tests were conducted in triplicate for each formulation.

Author contributions

Zhiwei Huang: conceptualisation; data curation; formal analysis; investigation; methodology; visualisation; writing original draft. Roman V. Moiseev: methodology; writing – review and editing. Solomon S. Melides: investigation. Wooli Bae: investigation; methodology. Izabela Jurewicz: conceptualisation; funding acquisition; supervision. Vitaliy V. Khutoryanskiy: funding acquisition; methodology; resources; supervision; writing – review and editing. Joseph L. Keddie: conceptualisation; funding acquisition; project administration; supervision; writing – review and editing.

Conflicts of interest

There are no conflicts to declare.

Acknowledgements

The authors acknowledge the China Scholarship Council (CSC 201906950049) and the Vice-Chancellor's Scholarship Fund of the University of Surrey for providing a PhD studentship for ZH. We thank Dr Agata Gajewicz-Jaromin for the TGA measurements. We thank Myrale Habel, Edgar Muñoz and Rosa Garriga for many helpful discussions. Funding for the transmission electron microscope was provided by an EPSRC Core Equipment grant (EP/V036327/1). VVK acknowledges the financial support provided by the European Union's Horizon 2020-MSCA-RISE-2018/823883: Soft Biocompatible Polymeric NANOstructures: A Toolbox for Novel Generation of Nano Pharmaceuticals in Ophthalmology (NanoPol) and also the Royal Society for a Royal Society Industry Fellowship (IF/R2/222031). VVK and RVM also acknowledge the University of Reading for the Early Stage Commercialisation Investment funding to set up Physicochemical, *Ex Vivo* and Invertebrates Tests and Analysis Centre (PEVITAC).

References

1 R. R. A. Bourne, J. D. Steinmetz, M. Saylan, A. M. Mersha, A. H. Weldemariam, T. G. Wondmeneh, C. T. Sreeramareddy, M. Pinheiro, M. Yaseri, C. Yu, M. S. Zastrozhin, A. Zastrozhina, Z. J. Zhang, S. R. M. Zimsen, N. Yonemoto, G. W. Tsegaye, G. T. Vu, A. Vongpradith, A. M. N. Renzaho and M. B. Sorrie, *et al.*, *Lancet Global Health*, 2021, **9**, e144–e160.

2 T. R. Fricke, N. Tahhan, S. Resnikoff, E. Papas, A. Burnett, S. M. Ho, T. Naduvilath and K. S. Naidoo, *Ophthalmology*, 2018, **125**, 1492–1499.

3 V. Gote, S. Sikder, J. Sicotte and D. Pal, *J. Pharmacol. Exp. Ther.*, 2019, **370**, 602–624.
4 I. K. Gipson, *Exp. Eye Res.*, 2004, **78**, 379–388.
5 E. Başaran and Y. Yazan, *Expert Opin. Drug Delivery*, 2012, **9**, 701–712.
6 Y. Zambito and G. Di Colo, *J. Drug Delivery Sci. Technol.*, 2010, **20**, 45–52.
7 C. C. Peng, L. C. Bengani, H. J. Jung, J. Leclerc, C. Gupta and A. Chauhan, *J. Drug Delivery Sci. Technol.*, 2011, **21**, 111–121.
8 A. L. Onugwu, C. S. Nwagwu, O. S. Onugwu, A. C. Echezona, C. P. Agbo, S. A. Ihim, P. Emeh, P. O. Nnamani, A. A. Attama and V. V. Khutoryanskiy, *J. Controlled Release*, 2023, **354**, 465–488.
9 N. Üstündag Okur, E. Ş. Çağlar and P. I. Siafaka, *J. Ocul. Pharmacol. Ther.*, 2020, **36**, 342–354.
10 R. K. Sahoo, N. Biswas, A. Guha, N. Sahoo and K. Kuotsu, *Biomed Res. Int.*, 2014, 1–12.
11 R. J. Marsh and D. M. Maurice, *Exp. Eye Res.*, 1971, **11**, 43–48.
12 B. B. Herlofson and P. Barkvoll, *Acta Odontol. Scand.*, 1994, **52**, 257–259.
13 M. A. R. Buzalaf, A. R. Hannas and M. T. Kato, *J. Appl. Oral Sci.*, 2012, **20**, 493–502.
14 A. Schrade, K. Landfester and U. Ziener, *Chem. Soc. Rev.*, 2013, **42**, 6823–6839.
15 Y. Chevalier and M. A. Bolzinger, *Colloids Surf., A*, 2013, **439**, 23–34.
16 W. Ramsden, *Proc. R. Soc.*, 1903, **72**, 156–164.
17 S. U. Pickering, *J. Chem. Soc., Trans.*, 1907, **91**, 2001–2021.
18 S. Simovic, N. Ghouchi-Eskandar and C. A. Prestidge, *J. Drug Delivery Sci. Technol.*, 2011, **21**, 123–133.
19 J. Marto, A. Ascenso, S. Simoes, A. J. Almeida and H. M. Ribeiro, *Expert Opin. Drug Delivery*, 2016, **13**, 1093–1107.
20 K. van der Laan, M. Hasani, T. Zheng and R. Schirhagl, *Small*, 2018, **14**, 1703838.
21 V. N. Mochalin, O. Shenderova, D. Ho and Y. Gogotsi, *Nat. Nanotechnol.*, 2012, **7**, 11–23.
22 Y. Zhu, J. Li, W. Li, Y. Zhang, X. Yang, N. Chen, Y. Sun, Y. Zhao, C. Fan and Q. Huang, *Theranostics*, 2012, **2**, 302–312.
23 R. Garriga, T. Herrero-Continente, M. Palos, V. L. Cebolla, J. Osada, E. Muñoz and M. J. Rodríguez-Yoldi, *Nanomaterials*, 2020, **10**, 1617.
24 A. M. Schrand, L. Dai, J. J. Schlager, S. M. Hussain and E. Osawa, *Diamond Relat. Mater.*, 2007, **16**, 2118–2123.
25 R. Kaur and I. Badea, *Int. J. Nanomedicine*, 2013, **8**, 203–220.
26 M. Ozawa, M. Inaguma, M. Takahashi, F. Kataoka, A. Krüger and E. Osawa, *Adv. Mater.*, 2007, **19**, 1201–1206.
27 A. Krueger, *Chem. – Eur. J.*, 2008, **14**, 1382–1390.
28 M. S. Ali, A. A. Metwally, R. H. Fahmy and R. Osman, *Int. J. Pharm.*, 2019, **558**, 165–176.
29 A. H. Day, S. J. Adams, L. Gines, O. A. Williams, B. R. G. Johnson, I. A. Fallis, E. J. Loveridge, G. S. Bahra, P. C. F. Oyston, J. M. Herrera and S. J. A. Pope, *Carbon*, 2019, **152**, 335–343.
30 A. Krueger and D. Lang, *Adv. Funct. Mater.*, 2012, **22**, 890–906.
31 N. M. Kuznetsov, S. I. Belousov, R. A. Kamyshinsky, A. L. Vasiliev, S. N. Chvalun, E. B. Yudina and A. Ya. Vul, *Carbon*, 2021, **174**, 138–147.
32 J. Beltz, A. Pfaff, I. M. Abdullahi, A. Cristea, V. N. Mochalin and N. Ercal, *Diamond Relat. Mater.*, 2019, **100**, 107590.
33 A. M. Vervald, E. N. Vervald, S. A. Burikov, S. V. Patsaeva, N. A. Kalyagina, N. E. Borisova, I. I. Vlasov, O. A. Shenderova and T. A. Dolenko, *J. Phys. Chem. C*, 2020, **124**, 4288–4298.
34 Z. Huang, I. Jurewicz, E. Muñoz, R. Garriga and J. L. Keddie, *J. Colloid Interface Sci.*, 2022, **608**, 2025–2038.
35 M. Garcia-Valldecabres, A. López-Alemany and M. F. Refojo, *Optometry*, 2004, **75**, 161–168.
36 M. Xiao, A. Xu, T. Zhang and L. Hong, *Front. Chem.*, 2018, **6**, 1–14.
37 D. Li, X. Sheng and B. Zhao, *J. Am. Chem. Soc.*, 2005, **127**, 6248–6256.
38 M. Motornov, R. Sheparovych, R. Lupitskyy, E. MacWilliams, O. Hoy, I. Luzinov and S. Minko, *Adv. Funct. Mater.*, 2007, **17**, 2307–2314.
39 N. Yandrapalli, T. Robinson, M. Antonietti and B. Kumru, *Small*, 2020, **16**, 1–7.
40 R. Garriga, I. Jurewicz, E. Romero, C. Jarne, V. L. Cebolla, A. B. Dalton and E. Muñoz, *ACS Appl. Mater. Interfaces*, 2016, **8**, 1913–1921.
41 R. Garriga, I. Jurewicz, S. Seyedin, N. Bardi, S. Totti, B. Matta-Domjan, E. G. Velliou, M. A. Alkhorayef, V. L. Cebolla, J. M. Razal, A. B. Dalton and E. Muñoz, *Nanoscale*, 2017, **9**, 7791–7804.
42 Z. Huang, E. Calicchia, I. Jurewicz, E. Muñoz, R. Garriga, G. Portale, B. J. Howlin and J. L. Keddie, *ACS Appl. Mater. Interfaces*, 2022, **14**, 53228–53240.
43 G. Celenza, R. Iorio, S. Cracchiolo, S. Petricca, C. Costagliola, B. Cinque, B. Segatore, G. Amicosante and P. Bellio, *Transl. Vis. Sci. Technol.*, 2020, **9**, 1–11.
44 J. Bart, R. Tiggelaar, M. Yang, S. Schlautmann, H. Zuilhof and H. Gardeniers, *Lab Chip*, 2009, **9**, 3481–3488.
45 A. J. Smith, F. I. Ali and D. V. Soldatov, *CrystEngComm*, 2014, **16**, 7196–7208.
46 G. Reina, L. Zhao, A. Bianco and N. Komatsu, *Angew. Chem., Int. Ed.*, 2019, **58**, 17918–17929.
47 J. S. Horsley, *South. Med. J.*, 1943, **36**, 8–12.
48 S. E. Kudaibergenov and A. Ciferri, *Macromol. Rapid Commun.*, 2007, **28**, 1969–1986.
49 V. N. Mochalin and Y. Gogotsi, *J. Am. Chem. Soc.*, 2009, **131**, 4594–4595.
50 N. Nunn, M. D'Amora, N. Prabhakar, A. M. Panich, N. Froumin, M. D. Torelli, I. Vlasov, P. Reineck, B. Gibson, J. M. Rosenholm, S. Giordani and O. Shenderova, *Methods Appl. Fluoresc.*, 2018, **6**, 1–10.
51 P. Reineck, D. W. M. Lau, E. R. Wilson, K. Fox, M. R. Field, C. Deeleepojananan, V. N. Mochalin and B. C. Gibson, *ACS Nano*, 2017, **11**, 10924–10934.
52 B. P. Binks and J. A. Rodrigues, *Langmuir*, 2007, **23**, 7436–7439.
53 C. Griffith and H. Daigle, *J. Colloid Interface Sci.*, 2018, **509**, 132–139.

54 W. J. Ganley and J. S. Van Duijneveldt, *Langmuir*, 2017, **33**, 1679–1686.
55 S. K. Wong, L. E. Low, J. Supramaniam, S. Manickam, T. W. Wong, C. H. Pang and S. Y. Tang, *Nanotechnol. Rev.*, 2021, **10**, 1293–1305.
56 B. V. Farias, D. Brown, A. Hearn, N. Nunn, O. Shenderova and S. A. Khan, *J. Colloid Interface Sci.*, 2020, **580**, 180–191.
57 N. J. Van Haeringen, *Surv. Ophthalmol.*, 1981, **26**, 84–96.
58 J. M. Tiffany, N. Winter and G. Bliss, *Curr. Eye Res.*, 1989, **8**, 507–515.
59 N. Dubashynskaya, D. Poshina, S. Raik, A. Urtti and Y. A. Skorik, *Pharmaceutics*, 2020, **12**, 1–30.
60 F. J. Otero-Espinar, A. Fernández-Ferreiro, M. González-Barcia, J. Blanco-Méndez and A. Luzardo, *Stimuli sensitive ocular drug delivery systems*, 2018.
61 H. Abdelkader, S. Ismail, A. Hussein, Z. Wu, R. Al-Kassas and R. G. Alany, *Int. J. Pharm.*, 2012, **432**, 1–10.
62 A. Schrage, S. N. Kolle, M. C. Rey Moreno, K. Norman, H. Raabe, R. Curren, B. Van Ravenzwaay and R. Landsiedel, *ATLA, Altern. Lab. Anim.*, 2011, **39**, 37–53.
63 M. H. Goldstein, F. Q. Silva, N. Blender, T. Tran and S. Vantipalli, *Eye*, 2022, **36**, 361–368.
64 S. Lee, D. Khun, G. L. Kumarasinghe, G. H. De Zoysa, V. Sarojini, H. R. Vellara, I. D. Rupenthal and S. S. Thakur, *Clin. Exp. Optom.*, 2019, **102**, 583–589.
65 B. A. Kerwin, *J. Pharm. Sci.*, 2008, **97**, 2924.
66 E. A. Mun, P. W. J. Morrison, A. C. Williams and V. V. Khutoryanskiy, *Mol. Pharm.*, 2014, **11**, 3556–3564.
67 R. V. Moiseev, P. W. J. Morrison, F. Steele and V. V. Khutoryanskiy, *Pharmaceutics*, 2019, **11**, 1–33.
68 P. W. J. Morrison and V. V. Khutoryanskiy, in *Fundamentals of Drug Delivery*, ed. H. A. E. Benson, M. S. Roberts, A. C. Williams and X. Liang, 2021, 1st edn, pp. 349–375.
69 V. V. Khutoryanskiy, *Macromol. Biosci.*, 2011, **11**, 748–764.
70 M. T. Cook, S. L. Smith and V. V. Khutoryanskiy, *Chem. Commun.*, 2015, **51**, 14447–14450.
71 G. S. Irmukhametova, G. A. Mun and V. V. Khutoryanskiy, *Langmuir*, 2011, **27**, 9551–9556.
72 S. Balakin, N. R. Dennison, B. Klemmed, J. Spohn, G. Cuniberti, L. Römhildt and J. Opitz, *Appl. Sci.*, 2019, **9**, 1064.
73 P. Facal Marina, J. Xu, X. Wu and H. Xu, *Chem. Sci.*, 2018, **9**, 4821–4829.
74 K. Kelley, *Multivariate Behav. Res.*, 2008, **43**, 524–555.
75 R. A. Cave, J. P. Cook, C. J. Connon and V. V. Khutoryanskiy, *Int. J. Pharm.*, 2012, **428**, 96–102.
76 R. V. Moiseev, F. Steele and V. V. Khutoryanskiy, *Pharmaceutics*, 2022, **14**, 1–20.
77 B. Srividya, R. M. Cardoza and P. D. Amin, *J. Controlled Release*, 2001, **73**, 205–211.

